Myxobacteria gliding motility requires cytoskeleton rotation powered by proton motive force

Beiyan Nan[a], Jing Chen[b], John C. Neu[c], Richard M. Berry[d], George Oster[a,1], and David R. Zusman[a,1]

Departments of [a]Molecular and Cell Biology and [c]Mathematics, and [b]Biophysics Graduate Group, University of California, Berkeley, CA 94720; and [d]Department of Physics, University of Oxford, Oxford OX1 3PU, United Kingdom

Contributed by George Oster, December 23, 2010 (sent for review November 4, 2010)

Myxococcus xanthus **is a Gram-negative bacterium that glides over surfaces without the aid of flagella. Two motility systems are used for locomotion: social-motility, powered by the retraction of type IV pili, and adventurous (A)-motility, powered by unknown mechanism(s). We have shown that AgmU, an A-motility protein, is part of a multiprotein complex that spans the inner membrane and periplasm of *M. xanthus*. In this paper, we present evidence that periplasmic AgmU decorates a looped continuous helix that rotates clockwise as cells glide forward, reversing its rotation when cells reverse polarity. Inhibitor studies showed that the AgmU helix rotation is driven by proton motive force (PMF) and depends on actin-like MreB cytoskeletal filaments. The AgmU motility complex was found to interact with MotAB homologs. Our data are consistent with a mechanochemical model in which PMF-driven motors, similar to bacterial flagella stator complexes, run along an endless looped helical track, driving rotation of the track; deformation of the cell surface by the AgmU-associated proteins creates pressure waves in the slime, pushing cells forward.**

Myxobacteria live in soil and have a complex life cycle that includes vegetative swarming, predation, and fruiting body formation. These activities are facilitated by two gliding motility systems: social (S)-motility and adventurous (A)-motility (1). S-motility is primarily involved in the movement of cells in groups and is powered by the retraction of type IV pili, similar to twitching motility in *Pseudomonas aeruginosa* (2–4). A-motility is required for the movement of isolated cells. Despite the identification of ≈40 A-motility related genes (5–7) and several intriguing hypotheses (8, 9), the mechanism of A-motility remains elusive.

We have been studying the motility mechanism in *Myxococcus xanthus* and the *frizzy* (Frz) chemosensory system that controls cell reversals. FrzCD, the chemoreceptor for the Frz pathway, contains an unusual N-terminal domain that interacts with two A-motility proteins: AglZ, a cytoplasmic protein, and AgmU, a protein that localizes to both the cytoplasm and periplasm (10, 11). *aglZ* and *agmU* mutants are defective in A-motility but show normal S-motility (11, 12). Cytoplasmic AgmU-mCherry colocalizes with AglZ-YFP (yellow fluorescent protein) in moving cells as distributed arrays of fluorescent clusters. Surprisingly, these clusters appear stationary as cells move forward (9, 11). Recently, we found that AgmU is also associated with many other A-motility proteins including AglT, AgmK, AgmX, AglW, and CglB. These proteins likely form a large multiprotein complex that spans the membrane and periplasm of the cells (11). Here, we report that periplasmic AgmU decorates a closed looped helix that rotates as cells move forward. Rotation depended on proton motive force (PMF) and an intact MreB cytoskeleton. Based on our findings, we propose a model of gliding motility in which MotAB homologs and associated motility proteins push against an endless looped helical track, driving the rotation of the track and the translocation of the cell.

Results and Discussion

Periplasmic AgmU Decorates a Looped Helix. To visualize periplasmic AgmU, we used a fluorescently labeled *agmU::mCherry* strain that showed no defects in motility or fruiting body formation (11). Fig. 1*A* shows deconvolved fluorescence images from a fixed cell; 3D reconstructions of AgmU:mCherry fluorescence from ≈20 images show that AgmU-mCherry forms a twisted endless looped helix that spans the length of the cells (Fig. 1*B*). The distance between adjacent nodes is 0.45 ± 0.09 μm (average of 10 cells), nearly identical to that of *M. xanthus* MreB helices, 0.47 ± 0.1 μm (13). Considering AgmU as a closed helical loop, the period of this helix is ≈0.7–1.1 μm.

AgmU-mCherry Helices Rotate as Cells Move on Hard Agar Surfaces. We also followed live *pilA*$^-$ *agmU-mCherry* (A^+S^- motile) cells by fluorescence video microscopy. We observed that the AgmU-mCherry helix rotates as cells move on a 1.5% agar surface and that the direction of rotation reverses when cells reverse their direction (Movies S1 and S2). Viewed from the lagging cell pole, the AgmU-mCherry helix always rotates clockwise. Additionally, the concentration of AgmU-mCherry is higher at the leading cell pole. When cells reverse, AgmU-mCherry relocalizes to the new leading cell pole within a few seconds (Fig. 1*C* and Movies S1 and S2). To exclude the possibility that the apparent rotational motion is an illusion caused by the uneven agar surface or the gliding motion itself, we suspended the *pilA*$^-$ *agmU::mCherry* cells in liquid culture or 1% methylcellulose solution and imaged the fluorescence at 2-s intervals. Without a surface for gliding, cells are stationary. Nevertheless, the AgmU-mCherry helical fluorescence continued to rotate as on agar surfaces (Movie S3). This rotation is illustrated in Fig. 1*D*, where the image of one frame (red; Fig. 1*D, Left*) is merged with a frame recorded 2 s later (green; Fig. 1*D, Middle*). During the 2-s time interval between images, the AgmU helix and the pitch remained unchanged, but the helix from each frame showed a clear shift compared with the previous frame (Fig. 1*D, Right*), consistent with rotation.

Because of the complexity of the images, we were unable to determine the rotational speed of the AgmU helices when viewed laterally. However, some cells in liquid culture or methylcellulose were perpendicular to the focal plane, yielding an end-on view. AgmU in these cells appeared as discontinuous circles because of changes in the depth of field, consistent with a looped helical structure. With this fluorescence discontinuity as a reference, we were able to determine the rotational speed of the AgmU helix by calculating the angular velocity of the discontinuity. Fig. 1*E* and Movie S4 show a rotational speed of ≈8.4 rpm; the average rotational speed from five individual cells was 7.5 ± 1.2 rpm. Because the AgmU helix shows a 0.7- to 1.1-μm period, the calculated linear velocity of cells would be ≈4.4–9.6 μm/min, consistent with the maximum velocity of A-motility, ≈2–4 μm/min

Author contributions: B.N., J.C., R.M.B., G.O., and D.R.Z. designed research; B.N., J.C., and R.M.B. performed research; B.N., J.C., J.C.N., R.M.B., and G.O. analyzed data; and B.N., J.C., G.O., and D.R.Z. wrote the paper.

The authors declare no conflict of interest.

[1]To whom correspondence may be addressed. E-mail: goster@berkeley.edu or zusman@berkeley.edu.

This article contains supporting information online at www.pnas.org/lookup/suppl/doi:10.1073/pnas.1018556108/-/DCSupplemental.

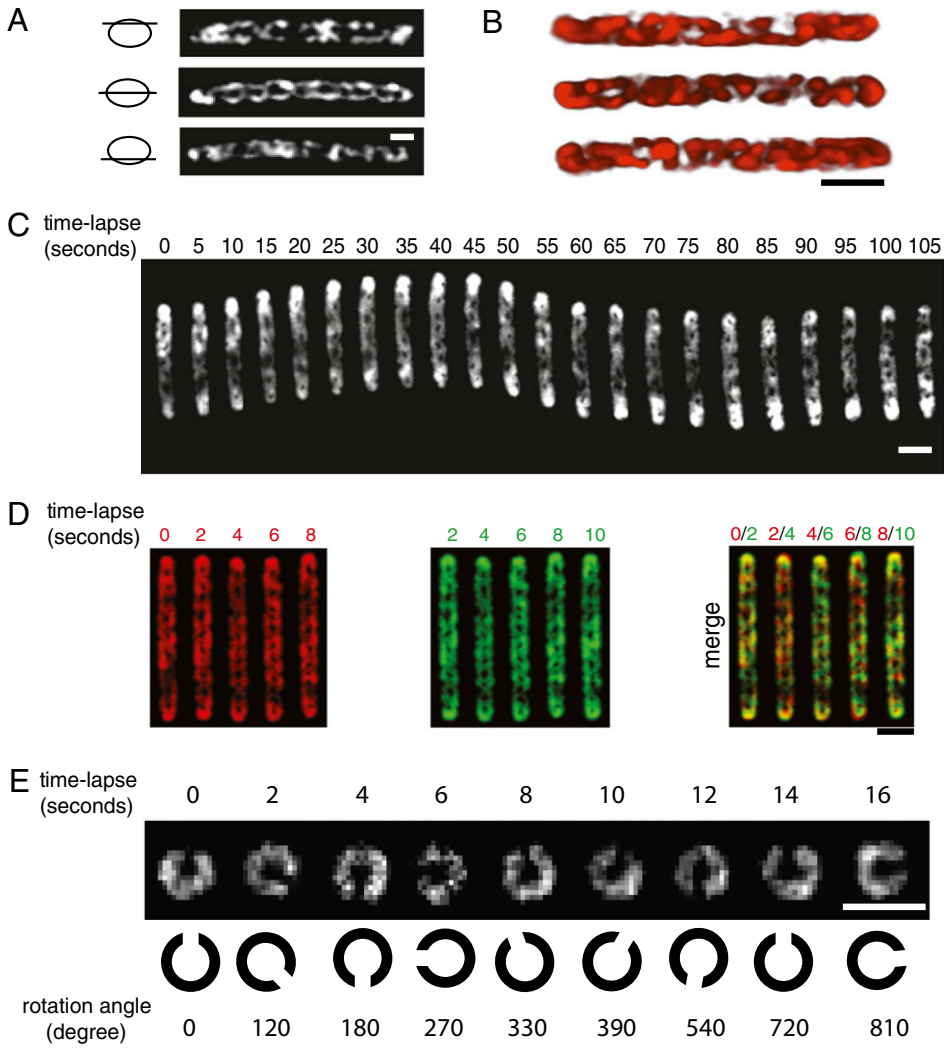

Fig. 1. Images of AgmU. (*A*) Deconvolved images of one fixed *agmU::mCherry* cell. (*B*) Three-dimensional reconstructions of the AgmU helix from three individual cells. (*C*) Time-lapse images of AgmU-mCherry in a moving cell. The bright clusters indicate the leading cell pole, which shifts to the opposite pole when cells reverse. (*D*) Time-lapse images of *agmU-mCherry pilA* cells in 1% methylcellulose. To visualize movement, one frame (red; *Left*) is merged (*Right* with a frame recorded 2 s later (green; *Center*). (*E*) Polar time-lapse views of an *agmU::mCherry pilA* cell in 1% methylcellulose. (Scale bars: 1 μm.)

(14). The helix may slip relative to the surface, or, alternatively, its rotation may be slower when the cell is associated with a surface.

Rotation of the AgmU Helix Is Driven by PMF. To determine the force driving the rotation of the AgmU helices, we followed the movement of cells and the rotation of AgmU helices in *pilA*$^-$ *agmU::mCherry* cells treated with carbonyl cyanide-m-chlorophenylhydrazone (CCCP, 20 μM, to disrupt the PMF) or sodium azide (NaN_3, 80 mM, to disrupt ATP synthesis). In the presence of azide, both gliding motility and helix rotation continued for at least 30 min (Movie S5). After 60 min, most cells stopped moving, although helix rotation continued (Movie S6). By contrast, CCCP treatment stopped motility and helix rotation within 5 min (Fig. 2*A* and Movie S7). CCCP functions as a proton carrier that discharges both the electric potential and the pH gradient of PMF. We therefore treated the *pilA*$^-$ *agmU::mCherry* cells with nigericin or valinomycin. Nigericin reduces the pH gradient across the membrane, whereas valinomycin acts as a K^+-ionophore, discharging the membrane potential. Fig. 2*B* and Movie S8 show that nigericin (100 μM) stopped both A-motility and the rotation of AgmU helices within 10 min, whereas valinomycin (50 μM, in the presence of 150 mM KCl) had no effect on A-motility or AgmU helix rotation, even after 1 h (Fig. 2*C* and Movie S9). These preliminary data show that the pH gradient across the membrane might be the major component of the PMF, which drives both A-motility and the rotation of the AgmU helices.

We used fluorescence recovery after photobleaching (FRAP) to determine whether individual AgmU molecules are fixed to the helix or move relative to it. *M. xanthus agmU::mCherry pilA* cells were photobleached by exposure to bright laser illumination, with a section near the middle of the cell (≈1 μm) protected from photobleaching. Fluorescence recovered along the length of the cell within ≈10 s in untreated cells (Fig. 2*D* and Movies S10 and S11), but did not recover even after 5 min in cells treated with 20 μM CCCP (Fig. 2*E* and Movies S12 and S13). Thus, AgmU molecules move up and down the cell along a helical track, and this movement depends on the PMF.

Rotation of the AgmU Helix Requires an Intact MreB Cytoskeleton. AgmU helices are similar in both pitch and conformation with the actin-like cytoskeleton protein MreB. To see whether AgmU rotation depends on the MreB cytoskeleton, we treated *pilA*$^-$ *agmU::mCherry* cells with 100 μg/mL A22, an inhibitor of MreB polymerization and motility in *M. xanthus* (13). At this concen-

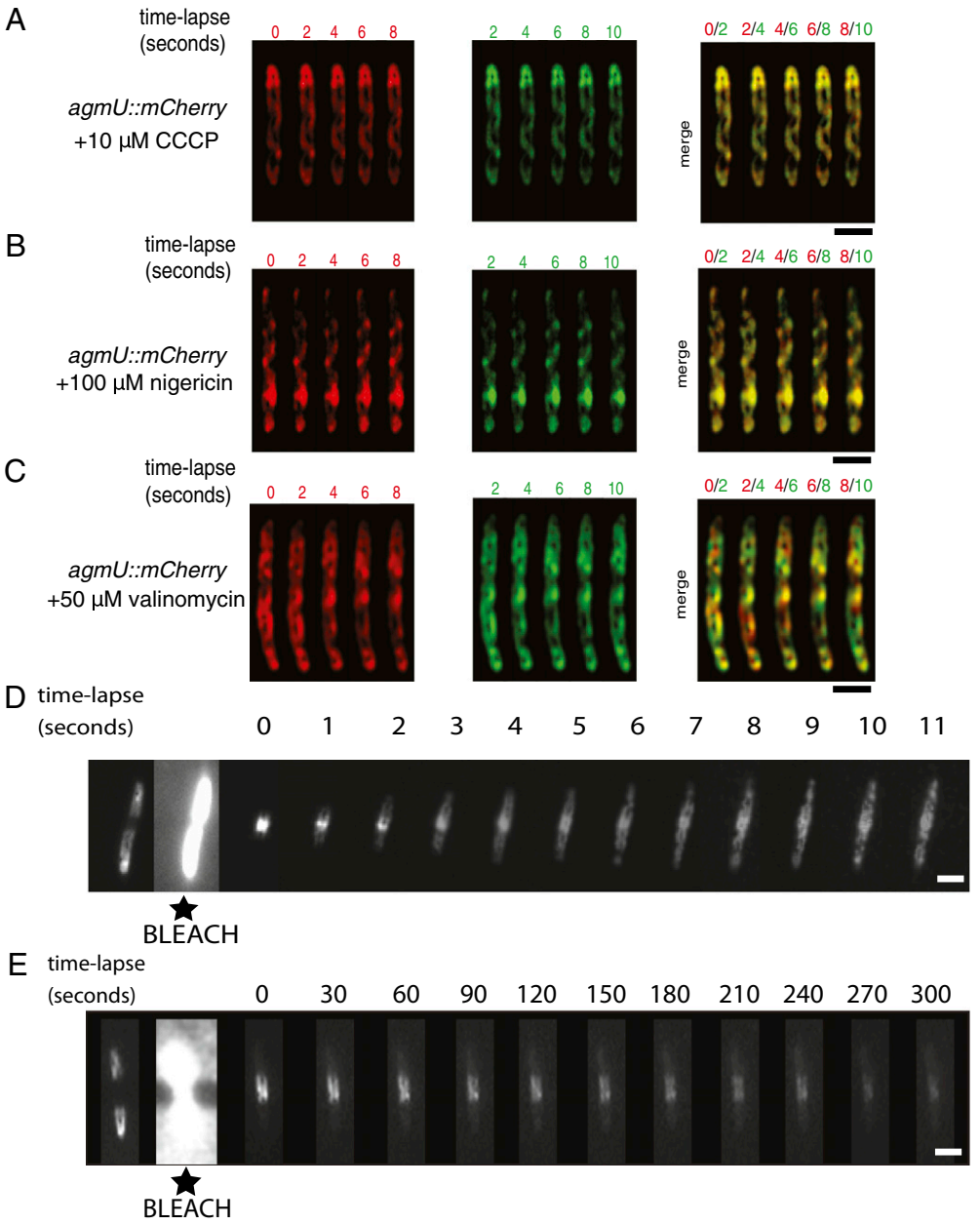

Fig. 2. The movements of the AgmU helix are powered by PMF. (*A–C*) Time-lapse images of *agmU-mCherry pilA* cells spotted on 1.5% agar containing CCCP (*A*), nigericin (*B*), or valinomycin (in the presence of 150 mM KCl) (*C*). Movements were visualized as in Fig. 1*D*. (*D* and *E*) FRAP. *agmU::mCherry pilA* cells were cultured in the absence (*D*) or presence (*E*) of CCCP. The cells were shielded with a ≈1-μm mask at their midsections and then bleached with a laser for 1 s. The recovery of fluorescence in the bleached cell poles was recorded at intervals. (Scale bars: 1 μm.)

tration, A22 abolished both A-motility and the rotation of AgmU within 10 min (Fig. 3*A* and Movie S14), whereas the helical localization pattern of AgmU remained largely unchanged. After longer incubation with A22 (>1 h), most of the cells lost their rod-like shape and the helical pattern of AgmU was disrupted (*SI Appendix*, Fig. S1*A*). A22 also prevented fluorescence recovery in FRAP experiments (Fig. 3*C* and Movie S15). By contrast, a strain carrying an A22-resistant mutation (*mreB*^{V323A}) (13) showed no defects in A-motility or AgmU helix rotation at a concentration of 200 μg/mL (Fig. 3*B* and Movie S16). NaN_3 treatment did not disrupt the MreB filaments (*SI Appendix*, Fig. S1 *B* and *C*). These data suggest that the MreB cytoskeleton is essential for the rotation of the AgmU helix. To investigate the possible involvement of peptidoglycan synthesis in the rotation of the AgmU helix, we treated the cells with cephalexin (100 μM, 8 h) or vancomycin (100 μM, 2 h). In both cases, no obvious change in the dynamics of AgmU was observed (Movies S17 and S18).

Cell Surface of *M. xanthus* Shows Helical Deformations That May Generate Translational Forces. We speculated that the associated A-motility proteins might distort the cell envelope and generate drag forces important for motility. We tested this prediction by total internal reflection fluorescence (TIRF) microscopy of *M. xanthus* cells expressing GFP in the cytoplasm (15). Cells were placed on glass microscope slides. TIRF images showed a modulation of intensity with a period of 0.85 ± 0.23 μm, similar to the periodicity of MreB helices and the other helical distributions of A-motility proteins reported above. Epifluorescence images

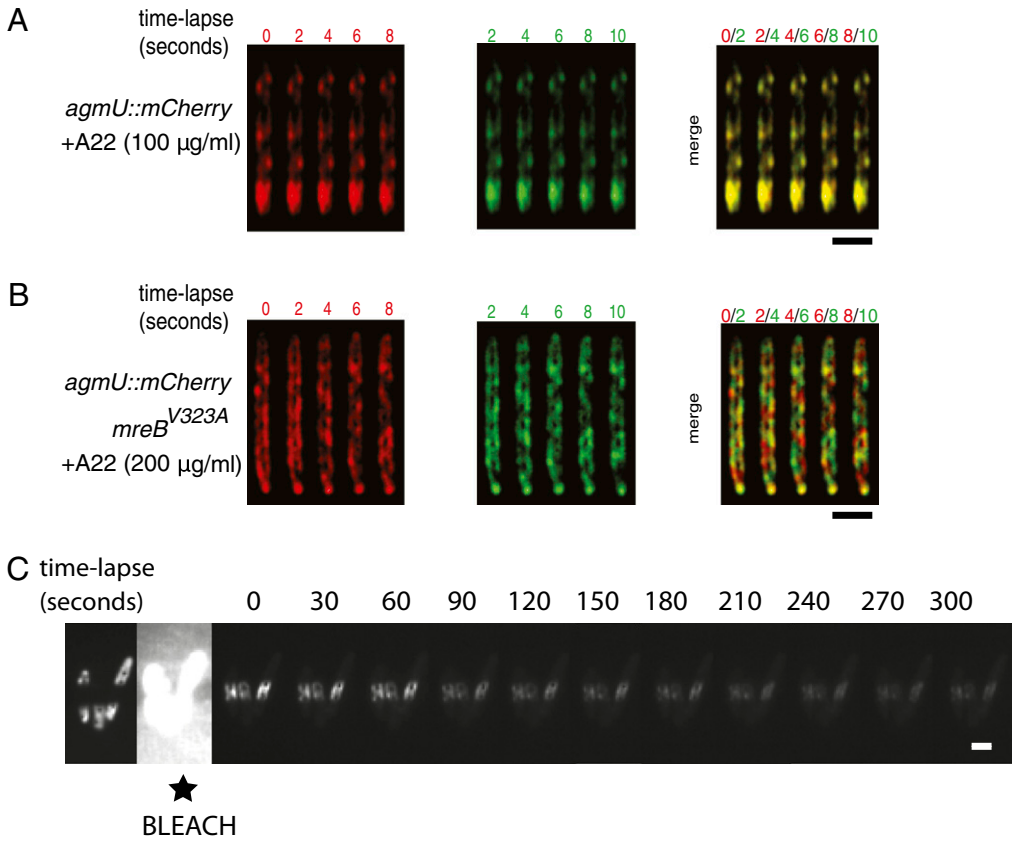

Fig. 3. AgmU helix movements require the MreB cytoskeleton. (*A* and *B*) Time-lapse images of *agmU::mCherry pilA* cells spotted on 1.5% agar containing A22. The rotation of the AgmU-mCherry helix stops after addition of A22 at 100 μg/mL (*A*). The rotation of AgmU-mCherry in cells carrying an A22-resistant mutation in the *mreB* gene (*mreB* ^{V323A}) is resistant to 200 μg/mL A22 (*B*). Movements were visualized as in Fig. 1*D*. (*C*) FRAP of *agmU::mCherry pilA* cells cultured in the presence (*C*) or absence (Fig. 2*D*) of A22 (100 μg/mL). FRAP experiments were performed as in Fig. 2 *D* and *E*. (Scale bars: 1 μm.)

showed GFP distributed evenly in the cytoplasm (Fig. 4). The TIRF images reflect periodic modulation of the distance between the cytoplasm and the glass. Thus, the presence of the helical track in the cell cytoplasm may be reflected in a helical contour on the surface of the cell, as observed by atomic force microscopy and scanning electron microscopy (16, 17).

MotAB Homologs Are Potential Candidates for A-Motility Motors. Flagella rotation is driven by motor proteins, MotAB, that use PMF to rotate the flagella filaments (18). We identified eight TolQ/TolR pairs in the *M. xanthus* genome that share homologies with MotA/MotB (19) (*SI Appendix*, Fig. S2). Two of the MotA/MotB pairs, AglX/AglV and AglR/AglS, were identified as essential for A-motility (5). We confirmed that *aglX* and *aglR* mutants show defects in A-motility (*SI Appendix*, Fig. S3). AglX and AglV proteins interact with each other and both interact with AgmU in affinity pull-down experiments (*SI Appendix*, Table S1). Additionally, AglX-mCherry and AglR-mCherry appear as rotating helices similar to AgmU (*SI Appendix*, Fig. S4 *A* and *B* and Movies S19 and S20), and their rotation is arrested by CCCP, nigericin, and A22 (*SI Appendix*, Fig. S4*C*). These results are consistent with a role for these MotA/MotB pairs in powering AgmU rotation and cell movement.

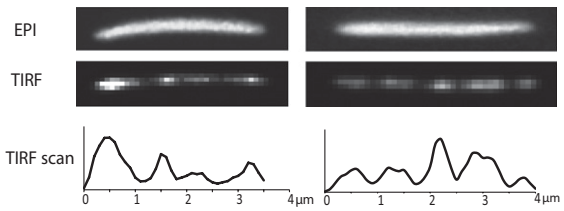

Fig. 4. Epifluorescence and TIRF microscopic images of cell surfaces. *M. xanthus* cells expressing GFP in the cytoplasm under the control of the *pilA* promoter were placed on glass microscope slides and imaged by epifluorescence and TIRF microscopy. Two typical cells are shown. The average distance between adjacent fluorescence peaks in the TIRF images is 0.85 ± 0.23 μm (calculated from 10 cells), similar to the periodicities of AgmU and MreB.

Helical Rotor Model for Gliding Motility. To explain our observations, we propose a mechanochemical model in which PMF-driven motor proteins (MotAB homologs) run along a looped helical track (Fig. 5*A*). The axial forces exerted by the motor drive the translocation of the cell, and the tangential forces drive the rotation of the track relative to the cell membrane, cell wall, and substrate.

Our model proposes that protein "cargos" associated with the motors induce different drag forces on the substrate (Fig. 5*B*). Motors carrying large, high-drag cargos constitute the major force-generating units in the system by distorting the cell surface and generating large drag forces against the substrate via the slime (Figs. 4 and 5*B*). As the motors carry the high-drag cargos through the ventral side of the track, the helically deformed contour of the cell surface pushes on the slime (Fig. 5*B*), causing a much larger drag on the motors than elsewhere. This increased drag causes the motors to collect in "traffic jams," creating equidistant, nearly stationary clusters. These clusters resemble those observed for AglZ and AgmU, presumably constituents of

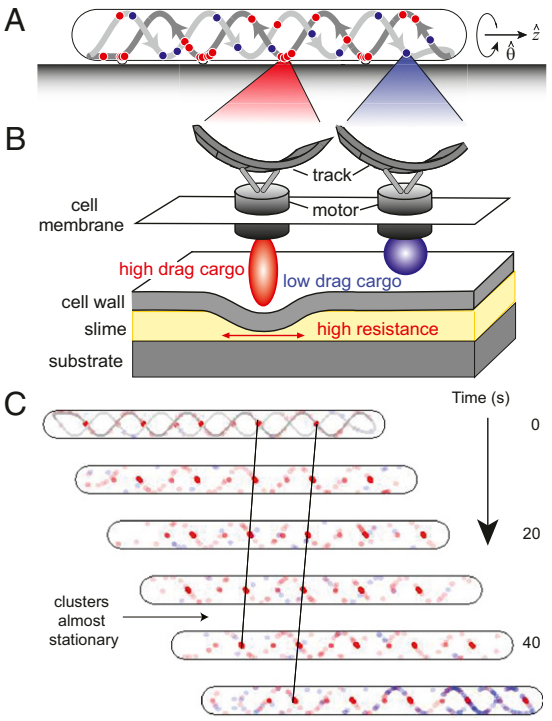

Fig. 5. Helical Rotor Model of gliding motility. (*A*) The motors push against the looped helical track (gray bands) in the same direction relative to the substrate; motors on opposite strands run in opposite directions (arrows along the bands). Blue dots are motors carrying small, low-drag cargo; red dots are motors carrying large, high-drag cargo. (*B*) Zoom-in view of the two types of motor–cargo complex. The high drag on the red cargo results from its bulky geometry, which deforms the cell envelope locally. The bump formed at the surface induces a high drag force on the motor. (*C*) Time-lapse snapshots of a computed cell viewed from the top (continuous movie, see Movie S21). The track is only shown in the first frame. The blue and red balls indicating the motors are semitransparent. When clustered, they look like one ball with brighter color. The motors carrying high-drag cargo slow down and form traffic jam clusters at the substrate interface where the external drag is highest (marked with arrows in *B*). The clusters are equally spaced by the pitch of the helical track. They move relative to the substrate much slower than the cell moves—in this computation, ≈0.4 μm/min. During the reversal, the motors carrying different cargo redistribute along the track. The cartoon compares well with the reported AglZ-GFP imaging experiments (9).

the high-drag cargo (Fig. 5*C* and Movie S21) (9, 11). In this view, the nearly stationary fluorescent patches are not "focal adhesions" in the sense of eukaryotic cell adhesions, but are aggregations of motors and cargos that provide the thrust driving gliding motility. Viewed externally, the motors driving the rotation of the helical rotor generate transverse waves on the ventral surface. These waves propagate toward the trailing pole and push on the substrate via the slime, analogous to a crawling snail (20). The low-drag cargos, although mechanically dispensable, explain the spatial localization of some other motility-related proteins, e.g., RomR, FrzCD, which may antagonize the localization of AglZ and AgmU.

Thus, in our model, the net driving force for cell movement results from the unequal distribution of high-drag vs. low-drag cargos loaded onto the motors running in opposite directions. These unequal distributions are determined by selective exchange of cargo as the motors reach the cell poles. The leading cell pole would preferentially load motors with high-drag cargos, whereas the trailing pole would load low-drag cargos. High-drag cargos are mostly traveling backward, generating net forward thrust. Cargo exchange may be controlled by an oscillator located at the cell poles that is linked to the Frz system. The oscillators are 180° out of phase because they are diffusively coupled [similar to the Min oscillator that controls cell division (21, 22)].

The model can be expressed as mechanical equations of motion (*SI Appendix*). Computer simulations of the equations reproduces the cell velocity (model 3.4 μm/min vs. experiment 2–4 μm/min) and track rotation speed of methycellulose-suspended cells (model 7.0 rpm vs. experiment 7.5 ± 1.2 rpm). The simulations show that the high-drag cargo clusters drift with a velocity ≈0.4 μm/min, too small to be distinguished experimentally.

The mechanochemical model explains the following features observed in experiments. (*i*) MotAB homologs, PMF, and MreB are all required for A-motility (the motors, powered by PMF, are predicted to move on cytoskeletal filaments); (*ii*) FRAP recovery of AgmU-mCherry is bidirectional (Movie S24) (motility proteins move in both directions because the cytoskeleton forms a closed loop); (*iii*) cells placed on soft agar, methylcellulose, or water cannot move but the AgmU helix keeps rotating (Movies S22 and S23) (There is little drag between the cargo and the super-soft external substrate and, therefore, little axial thrust. But internal drag forces between the motor, cell membrane, and cell wall remain, and they drive the rotation of the track. Detailed explanation in the *SI Appendix*.); (*iv*) cells on hard surfaces, like glass, show brighter AgmU clusters (11) (hard surfaces cause the motor proteins to slow down even more and make stronger traffic jams where the surface distortions meet the substrate); (*v*) the ≈7-min periodic reversal of cells (23, 24) (this is set by the period of the polar chemical oscillators); (*vi*) the preferential distribution of AglZ at the leading pole, as synchronized with cell reversals (9), versus RomR at the lagging pole (25) (the two proteins are assumed to be the high and low drag cargos, respectively); and (*vii*) the phenomenon of "elasticotaxis" where cells tend to orient along strain lines in the substrate (23). Details of the model and calculations are presented in *SI Appendix* and Movies S21, S22, S23, and S24.

We speculate that a similar motility mechanism may be widespread in bacteria because MreB and MotA/MotB homologs are common across a variety of bacterial species. For example, the abundant swimming cyanobacterium, *Synechococcus*, rotates about its long axis after it hits a wall, establishing a rotational component in the motility. This motion could be realized by a rotating helical track with motors running along it or motors anchored to the peptidoglycan layer driving the helical track. If the cell surface assumes a helical pattern because of the interior helix, the helix rotation would be reflected in helical waves on the surface that provide axial thrust and rotational torque (26, 27). Variations on this proposed motility mechanism could explain the behavior of other gliding bacteria such as *Cytophaga* sp. strain U67, which moves 60 times faster on glass surfaces than *M. xanthus.* An internal rotating helix could explain how latex spheres run up one side and down the other, and the observation that gliding is punctated by bouts of conical rotation about its leading pole similar to *Synechococcus* (28).

Materials and Methods

Bacterial Strains and Growth Conditions. Strains and plasmids used in this study are listed in *SI Appendix*, Table S2. *M. xanthus* strains were cultured in CYE medium, which contains 10 mM Mops at pH 7.6, 1% (wt/vol) Bacto Casitone (BD Biosciences), 0.5% Bacto yeast extract and 4 mM $MgSO_4$ (29). Five-microliter 4×10^8 cfu·ml^{-1} vegetative cultures were subjected to microscope observation directly (for the observation of cells suspended in liquid culture) or mixed with 200 μL of 1% (wt/vol) methylcellulose solution and spotted into a silicon gasket (for the observation of cells suspended in methylcellulose solution) or spotted on a thin layer of 1/2 CTT agar pad containing 1.5% (wt/vol) agar (30) (for the observation of cells gliding on agar). GST-tagged copurification and mass spectrometry were performed as described (11).

Microscopic Studies. Time-lapse and deconvolution fluorescence microscopy was performed as described (10, 11). Three-dimensional reconstructions of deconvolution images were performed with Imaris software (Bitplane). TIRF images were recorded at 2 Hz in frame-transfer mode with an electron-

multiplier gain setting of 2. FRAP images of the untreated, CCCP, and A22-treated cells were recorded at 2, 0.3, and 0.2 Hz, respectively, in frame-transfer mode with an electron-multiplier gain setting of 2. Fluorescence emission was imaged at ≈133 nm per pixel. For TIRF experiments, the distortion of cell envelope was monitored by cytoplasmic GFP expressed under the control of the *pilA* promoter (15).

ACKNOWLEDGMENTS. We thank T. Mignot, J. Shaevitz, and M. Sun for helpful discussions and sharing of recent data; J. Liphardt for providing microscope facility and valuable suggestions; L. Kohlstaedt and D. Mavrici for their help with mass spectrometry; and I.-H. Sun and L. Pan for their help with strain construction. B.N. and D.R.Z. were supported by National Institutes of Health Grant GM20509, and J.C. and G.O. were supported by National Science Foundation Grant DMS 0414039.

1. Hodgkin J, Kaiser D (1979) Genetics of gliding motility in *Myxococcus xanthus* (myxobacterales): Two gene systems control movement. *Mol Gen Genet* 171:177–191.
2. Henrichsen J (1972) Bacterial surface translocation: A survey and a classification. *Bacteriol Rev* 36:478–503.
3. Sun H, Zusman DR, Shi W (2000) Type IV pilus of *Myxococcus xanthus* is a motility apparatus controlled by the *frz* chemosensory system. *Curr Biol* 10:1143–1146.
4. Li Y, et al. (2003) Extracellular polysaccharides mediate pilus retraction during social motility of *Myxococcus xanthus*. *Proc Natl Acad Sci USA* 100:5443–5448.
5. Youderian P, Burke N, White DJ, Hartzell PL (2003) Identification of genes required for adventurous gliding motility in *Myxococcus xanthus* with the transposable element mariner. *Mol Microbiol* 49:555–570.
6. Yu R, Kaiser D (2007) Gliding motility and polarized slime secretion. *Mol Microbiol* 63: 454–467.
7. Hartzell P, Shi W, Youderian P (2008) *Gliding Motility of Myxococcus xanthus. Myxobacteria: Multicellularity and Differentiation*, ed Whitworth DE (Am Soc Microbiol, Washington, DC), pp 103–122.
8. Wolgemuth C, Hoiczyk E, Kaiser D, Oster G (2002) How myxobacteria glide. *Curr Biol* 12:369–377.
9. Mignot T, Shaevitz JW, Hartzell PL, Zusman DR (2007) Evidence that focal adhesion complexes power bacterial gliding motility. *Science* 315:853–856.
10. Mauriello EMF, Nan B, Zusman DR (2009) AglZ regulates adventurous (A-) motility in *Myxococcus xanthus* through its interaction with the cytoplasmic receptor, FrzCD. *Mol Microbiol* 72:964–977.
11. Nan B, Mauriello EMF, Sun IH, Wong A, Zusman DR (2010) A multi-protein complex from *Myxococcus xanthus* required for bacterial gliding motility. *Mol Microbiol* 76: 1539–1554.
12. Yang R, et al. (2004) AglZ is a filament-forming coiled-coil protein required for adventurous gliding motility of *Myxococcus xanthus*. *J Bacteriol* 186:6168–6178.
13. Mauriello EMF, et al. (2010) Bacterial motility complexes require the actin-like protein, MreB and the Ras homologue, MglA. *EMBO J* 29:315–326.
14. Sun H, Yang Z, Shi W (1999) Effect of cellular filamentation on adventurous and social gliding motility of *Myxococcus xanthus*. *Proc Natl Acad Sci USA* 96: 15178–15183.
15. Berleman JE, Scott J, Chumley T, Kirby JR (2008) Predataxis behavior in *Myxococcus xanthus*. *Proc Natl Acad Sci USA* 105:17127–17132.
16. Pelling AE, Li Y, Shi W, Gimzewski JK (2005) Nanoscale visualization and characterization of *Myxococcus xanthus* cells with atomic force microscopy. *Proc Natl Acad Sci USA* 102:6484–6489.
17. Lünsdorf H, Schairer HU (2001) Frozen motion of gliding bacteria outlines inherent features of the motility apparatus. *Microbiology* 147:939–947.
18. Minamino T, Imada K, Namba K (2008) Molecular motors of the bacterial flagella. *Curr Opin Struct Biol* 18:693–701.
19. Cascales E, Lloubès R, Sturgis JN (2001) The TolQ-TolR proteins energize TolA and share homologies with the flagellar motor proteins MotA-MotB. *Mol Microbiol* 42: 795–807.
20. Chan B, Balmforth NJ, Hosoi AE (2005) Building a better snail: Lubrication and adhesive locomotion. *Phys Fluids* 17:113101–113110.
21. Howard M, Kruse K (2005) Cellular organization by self-organization: Mechanisms and models for Min protein dynamics. *J Cell Biol* 168:533–536.
22. Howard M, Rutenberg AD, de Vet S (2001) Dynamic compartmentalization of bacteria: Accurate division in *E. coli*. *Phys Rev Lett* 87:278102.
23. Mauriello EM, Mignot T, Yang Z, Zusman DR (2010) Gliding motility revisited: How do the myxobacteria move without flagella? *Microbiol Mol Biol Rev* 74:229–249.
24. Zusman DR, Scott AE, Yang Z, Kirby JR (2007) Chemosensory pathways, motility and development in *Myxococcus xanthus*. *Nat Rev Microbiol* 5:862–872.
25. Leonardy S, Freymark G, Hebener S, Ellehauge E, Søgaard-Andersen L (2007) Coupling of protein localization and cell movements by a dynamically localized response regulator in *Myxococcus xanthus*. *EMBO J* 26:4433–4444.
26. Stone HA, Samuel AD (1996) Propulsion of microorganisms by surface distortions. *Phys Rev Lett* 77:4102–4104.
27. Ehlers KM, Samuel AD, Berg HC, Montgomery R (1996) Do cyanobacteria swim using traveling surface waves? *Proc Natl Acad Sci USA* 93:8340–8343.
28. Lapidus IR, Berg HC (1982) Gliding motility of *Cytophaga* sp. strain U67. *J Bacteriol* 151:384–398.
29. Campos JM, Geisselsoder J, Zusman DR (1978) Isolation of bacteriophage MX4, a generalized transducing phage for *Myxococcus xanthus*. *J Mol Biol* 119:167–178.
30. Wu SS, Kaiser D (1997) Regulation of expression of the *pilA* gene in *Myxococcus xanthus*. *J Bacteriol* 179:7748–7758.